

Radar Backscatter Measurement Accuracies Using Digital Doppler Processors in Spaceborne Scatterometers

CHONG-YUNG CHI, MEMBER, IEEE, DAVID G. LONG, AND FUK-KWOK LI, MEMBER, IEEE

Abstract—The normalized standard deviation, K_p , of radar backscatter measurements using digital Doppler processors in spaceborne scatterometers is derived. The K_p expression for analog Doppler filter processors, such as that used in the Seasat scatterometer [7] is shown to be a special case of the derived K_p expression. A connection to Welch's power spectrum estimation results [6] is also made. Tradeoff studies in digital filter design such as hardware complexity, computational speed, and system performance can be performed based on this K_p expression. We briefly discuss a current application in the design of the NASA scatterometer (NSCAT) to be flown in 1990. This derivation should be useful for system design and analysis of other radar remote-sensing instruments.

I. INTRODUCTION

A SCATTEROMETER is a radar system that measures the normalized scattering coefficient σ_0 of an illuminated surface by measuring the return signal power of a radar backscatter signal [1]. Scatterometers have been flown on the spaceborne platforms Skylab and Seasat. The Seasat scatterometer (SASS) demonstrated the ability to infer wind speed and direction over the ocean from σ_0 measurements [2], [3]. Using the radar equation and the measured return signal power P_r , σ_0 can be computed using the well-known radar equation

$$\sigma_0 = \frac{(4\pi)^3 R^4 P_r}{P_t G^2 \lambda^2 A L} \quad (1)$$

where

- P_t is the transmitted signal power;
- G is the antenna gain;
- λ is the wavelength of the signal;
- A is the Doppler cell area;
- R is the slant range to the illuminated Doppler cell; and
- L is the system loss.

SASS used four dual-polarized (vertical and horizontal polarizations) fan-beam antennas pointed at 45° and 135° relative to the spacecraft flight direction to produce an X-shaped illumination pattern on the Earth. In this way a

Manuscript received April 15, 1985; revised October 4, 1985. The research described in this paper was performed by the Jet Propulsion Laboratory, California Institute of Technology, under contract with NASA.

The authors are with the Jet Propulsion Laboratory, California Institute of Technology, Pasadena, CA 91109.

IEEE Log Number 8607907.

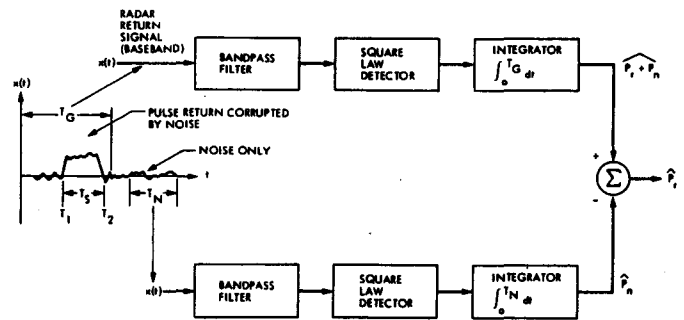


Fig. 1. Signal processing system for a scatterometer using analog filters.

given surface location was first viewed by a forward-looking antenna, and then viewed by an aft-looking antenna some time later. A train of microwave pulses was transmitted to the Earth's surface. The reflected signal for each pulse was Doppler shifted due to relative motion of the spaceborne scatterometer with respect to the Earth's surface. Signals from different locations in the antenna illumination pattern will have different Doppler shifts, and, by separating the return signal in the Doppler spectral domain, the desired along-beam resolution can be achieved. We will refer to each of the Doppler-shifted resolution cells as a " σ_0 cell."

SASS utilized analog devices for signal power estimates. These consisted of bandpass filters, square-law detectors, and gated integrators (see Fig. 1). The fixed frequency bands used in the bandpass filters caused radar system performance degradation in several areas. The Doppler shifts induced by the Earth's rotation caused the locations of the σ_0 cells of the forward-looking antenna beams to shift relative to those of the aft looking beams. This led to a loss in swath coverage as well as misregistration of the σ_0 cells. The misregistration could produce errors in the inferred wind vectors when wind gradients are present. A solution to these problems is to use a digital signal processor in which the frequency bands of the σ_0 cells can be adjusted to compensate for the Earth's rotation.

Such a digital processor is planned for use on the NASA scatterometer (NSCAT) to be flown in 1990 [4], [5]. The fast Fourier transform (FFT)-based digital processor allows the Doppler frequencies of σ_0 cells to be adjusted in order to maintain nearly constant cross-track distances

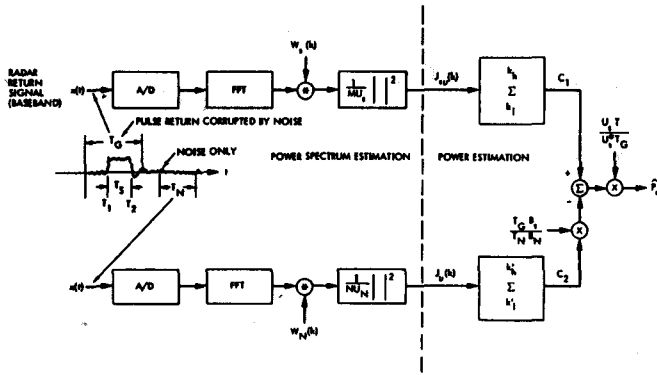


Fig. 2. Signal processing system for a scatterometer using FFT-based digital processing.

from the spacecraft ground track for the σ_0 cells. An additional advantage of the FFT-based digital processing scheme is that the Doppler center frequency and bandwidth of the σ_0 cells can be readily modified to compensate for slight variations in orbital parameters due to launch errors or in-orbit maneuvers.

A schematic diagram of the NSCAT digital processing technique is shown in Fig. 2. The scatterometer return signal is passed through the top path to estimate the power C_1 of the signal plus noise. A separate measurement is made using the bottom path to estimate the noise power, C_2 alone. Both of these measurements are telemetered to ground for further processing. In the ground data processing, an unbiased estimate of the backscatter power P_r is obtained by a linear combination of C_1 and C_2 .

Each path in Fig. 2 consists of the following on-board instrument functions: a) computation of the FFT, b) application of a window by convolution, c) squaring for power detection, and d) computation of the signal power within a σ_0 cell by summing the result of c) over the frequency bins corresponding to the range of Doppler frequencies of that σ_0 cell. In effect, a), b), and c) provide Welch's power spectrum estimates [6] of the scatterometer return signal, and d) acts as a bandpass filter. During ground processing the unbiased estimate of P_r is then used to determine the radar backscatter cross section σ_0 .

Data windowing is used in step b) to reduce spectral leakage. This reduces any bias in the estimated signal power caused by "interference" between σ_0 cells. This interference can be severe in situations where there are large variations in the power spectrum of the return signal, such as in the case of a strong wind gradient over the ocean. Although the variance of Welch's spectrum estimate has little dependence on the window itself, the variance of the power estimate over a frequency band may increase due to correlation between frequency bins caused by windowing. Thus, windowing may adversely affect the accuracy of the signal power estimate. In order to minimize this degradation in the power estimate accuracy, temporal-domain overlapped processing of the FFT data segments is used in step c).

A commonly adopted parameter for evaluating the performance of spaceborne scatterometers is the so-called K_p

parameter [7]. It is defined to be the normalized standard deviation of the measured σ_0 , $\hat{\sigma}_0$, i.e.

$$K_p = \frac{\{\text{Var}[\hat{\sigma}_0]\}^{1/2}}{\sigma_0} \quad (2)$$

where $\text{Var}[\hat{\sigma}_0]$ is the variance of $\hat{\sigma}_0$. The smaller the value of K_p , the better the estimate of σ_0 is. A general goal in scatterometer design is to minimize K_p .

The K_p equation for an analog signal power estimator, such as that used on SASS, was derived by Fisher [7]. In this paper, we derive the K_p equation for the digital signal processor shown in Fig. 2. The derived expression for K_p , which is more complicated than that for the analog case, is being used to make processor design and performance tradeoffs for NSCAT. We feel that this derivation should be useful for system design and analysis of other radar remote sensing instruments.

In Section II, we briefly review Welch's power spectrum estimation. The expression for K_p is then derived in detail in Section III. Two illustrative examples are described in Section IV. Finally, we briefly discuss the utility of this equation in scatterometer system design in Section V.

II. MEAN AND COVARIANCE OF WELCH'S POWER SPECTRUM ESTIMATION FOR STATIONARY GAUSSIAN PROCESSES

In subsequent analysis, we will frequently use the mean and covariance of Welch's power spectral estimation for stationary Gaussian processes. The expressions for mean and variance can be found in [6]. The covariance, however, is not commonly found in the literature. In this section, we briefly describe the expression for the covariance. Details of the derivation are shown in Appendix I.

Let $x(n)$, $n = 0, 1, 2, \dots, L-1$ be the given real data set sampled from a zero-mean stationary Gaussian random process with power spectral density (psd) $P_x(\omega)$. Segments of these sampled data, possibly overlapping, of length M with starting points of the segments D units apart are constructed. Assuming that we have K such segments $x_i(n)$, $i = 1, 2, \dots, K$ that cover the entire record. Then $x_i(n)$ is given by

$$x_i(n) = \begin{cases} x(n + (i-1)D), & 0 \leq n \leq M-1 \\ 0, & \text{otherwise} \end{cases} \quad (3)$$

with $(K-1)D + M = L$. The modified periodogram for each segment is defined as [6], [8]

$$\begin{aligned} J_i(\omega) &= \frac{1}{MU_i} \left| \sum_{n=0}^{M-1} x_i(n) \gamma_i(n) e^{-j\omega n} \right|^2 \\ &= \frac{1}{MU_i} |X_i(\omega) * \Gamma_i(\omega)|^2 \end{aligned} \quad (4)$$

where $X_i(\omega)$ and $\Gamma_i(\omega)$ are the Fourier transform of $x_i(n)$ and the data window $\gamma_i(n)$, respectively, and

$$U_i = \frac{1}{M} \sum_{n=0}^{M-1} \gamma_i^2(n). \quad (5)$$

The Welch's power spectrum estimate, $J(\omega)$, is defined as [6], [8]

$$J(\omega) = \frac{1}{K} \sum_{i=1}^K J_i(\omega). \quad (6)$$

Let us assume that the bandwidths of the windows $\gamma_i(n)$ and $\gamma_{ij}(n)$ are narrow compared to the variations of the power spectrum $P_x(\omega)$ where

$$\gamma_{ij}(n) = \gamma_i(n) \gamma_j(n + (i - j) D). \quad (7)$$

Finally, we assume that

$$|\Gamma_{ij}(\omega_1 - \omega_2)|^2 \gg |\Gamma_{ij}(\omega_1 + \omega_2)|^2, \quad (8)$$

for all $\omega_1, \omega_2 \in (\omega_a, \omega_b)$.

(Note that the value of $P_x(\omega)$ outside (ω_a, ω_b) is not needed in the following discussion.)

Assuming that $P_x(\omega)$ is constant over the frequency band (ω_a, ω_b) , i.e.

$$P_x(\omega) = P, \quad \text{for all } \omega \in (\omega_a, \omega_b) \quad (9)$$

then one can easily show that [6], [8]

$$\begin{aligned} E[J(\omega)] &= E[J_i(\omega)] \\ &= \frac{1}{MU_i} \frac{1}{2\pi} \int_{-\pi}^{\pi} P_x(\theta) |\Gamma_i(\omega - \theta)|^2 d\theta \\ &= \left(\frac{1}{MU_i}\right) \left(\frac{1}{2\pi}\right) P \\ &\quad \int_{-\pi}^{\pi} |\Gamma_i(\omega - \theta)|^2 d\theta = P \quad \forall \omega \in (\omega_a, \omega_b). \end{aligned} \quad (10)$$

The autocovariance function of $J(\omega)$, as derived in Appendix I, is given by

$$\begin{aligned} \text{Cov} \{J(\omega_1), J(\omega_2)\} \\ &= \frac{1}{K^2} \frac{P^2}{M^2} \sum_{i=1}^K \sum_{j=1}^K \left(\frac{1}{U_i U_j}\right) |\Gamma_{ij}(\omega_1 - \omega_2)|^2 \\ &\quad \forall \omega_1, \omega_2 \in (\omega_a, \omega_b). \end{aligned} \quad (11)$$

III. DERIVATION OF K_p

From (1) and (2), K_p can be expressed as

$$K_p = \frac{\{\text{Var} [\hat{P}_r]\}^{1/2}}{P_r} \quad (12)$$

where \hat{P}_r is the output of the signal power estimator in Fig. 2 and $\text{Var} [\hat{P}_r]$ is its variance.

From Fig. 2, one can see that the scatterometer received signal $x(t)$ can be modeled as

$$x(t) = s(t) \text{rect}(t - T_1) + \nu(t) \quad (13)$$

where

$$\text{rect}(t) = \begin{cases} 1, & 0 < t < T_s \\ 0, & \text{otherwise} \end{cases} \quad (14)$$

$s(t)$ is the returned signal, T_1 and T_s are the starting time and the pulse length of the received signal, respectively, and $\nu(t)$ is noise. We assume that the scatterometer signal from the Earth's surface can be modeled as a stationary bandlimited Gaussian process (see [1]).

$$P_s(f) = 0, \quad \text{for } |f| > f_s/2 \quad (15)$$

where f_s is the Nyquist sampling frequency. The noise $\nu(t)$ is assumed to be a stationary Gaussian process with zero mean and power spectral density

$$P_\nu(f) = b, \quad \text{for } |f| < f_s/2 \quad (16)$$

i.e., $P_\nu(f)$ is constant over all the frequency range. Furthermore, we assume that

$$P_s(f) = P_r/B_s, \quad \text{for } f_l \leq f \leq f_h = f_l + B_s \quad (17)$$

where P_r is the power of $s(t)$ over the frequency range (f_l, f_h) and B_s is the bandwidth used for a given σ_0 cell. Thus, the psd's for $s(n)$ and $\nu(n)$ are

$$P_s(\omega) = \frac{b}{T}, \quad 0 \leq \omega < 2\pi \quad (18)$$

$$P_\nu(\omega) = \frac{P_r}{B_s T}, \quad \omega_l \leq \omega \leq \omega_h \quad (19)$$

where $\omega_h = 2\pi f_h T$, $\omega_l = 2\pi f_l T$ and $T = 1/f_s$.

The derivation of the K_p expression for the system shown in Fig. 2 is performed in three steps. First, the mean and variance of the output C_1 of the top path in Fig. 2 are derived. Second, the mean and variance of the output C_2 of the bottom path in Fig. 2 are derived. Finally, the unbiased estimate \hat{P}_r of P_r , obtained by a linear combination of C_1 and C_2 , and its normalized standard deviation, K_p , are derived. These steps are shown in the following subsections.

We assume that the number of data segments, the number of data points in each segment and the window function are K_1 , M , and $w_s(n)$ for the top path and K_2 , N , and $w_N(n)$ for the bottom path in Fig. 2. We also assume that $D = D_1$ and $D = D_2$ for the top and bottom paths, respectively. First, we concentrate on the mean and variance of C_1 .

A. Mean and Variance of C_1

Welch's spectrum estimate for the top (signal plus noise) path in Fig. 2 that contains K_1 data segment overlapping $M-D$ points is given by

$$J_{sv}(\omega) = \frac{1}{K_1} \sum_{i=1}^{K_1} J_{sv_i}(\omega) \quad (20)$$

where

$$J_{sv_i}(\omega) = \frac{1}{MU_s} \left| \sum_{n=0}^{M-1} x_i(n) w_s(n) e^{-j\omega n} \right|^2 \quad (21)$$

with

$$U_s = \frac{1}{M} \sum_{n=0}^{M-1} w_s^2(n). \quad (22)$$

We can express $x_i(n) w_s(n)$ as (see (13))

$$x_i(n) w_s(n) = x_{s_i}(n) + x_{v_i}(n) \quad (23)$$

where

$$x_{v_i}(n) = v_i(n) w_s(n) = v(n + (i-1)D_1) w_s(n) \quad (24)$$

$$x_{s_i}(n) = s(n + (i-1)D_1) \gamma_i(n) \quad (25)$$

with

$$\gamma_i(n) = \begin{cases} \text{rect}(nT + (i-1)D_1T - T_1) w_s(n), \\ 0 \leq n \leq M-1 \\ 0, \text{ otherwise.} \end{cases} \quad (26)$$

From (21) and (23) we have

$$J_{s_{v_i}}(\omega) = \left(\frac{U_i}{U_s}\right) J_{s_i}(\omega) + J_{v_i}(\omega) + \frac{1}{MU_s} [X_{s_i}(\omega) X_{v_i}^*(\omega) + X_{s_i}^*(\omega) X_{v_i}(\omega)] \quad (27)$$

where

$$J_{s_i}(\omega) = \left(\frac{1}{MU_i}\right) \left| \sum_{n=0}^{M-1} x_{s_i}(n) e^{-j\omega n} \right|^2 = \left(\frac{1}{MU_i}\right) |X_{s_i}(\omega)|^2 \quad (28)$$

and

$$J_{v_i}(\omega) = \left(\frac{1}{MU_s}\right) \left| \sum_{n=0}^{M-1} x_{v_i}(n) e^{-j\omega n} \right|^2 = \frac{1}{MU_s} |X_{v_i}(\omega)|^2. \quad (29)$$

From (20) and (27) we get

$$J_s(\omega) = J_s(\omega) + J_v(\omega) + I_{s_v}(\omega) \quad (30)$$

where

$$J_s(\omega) = \frac{1}{U_s K_1} \sum_{i=1}^{K_1} U_i J_{s_i}(\omega) \quad (31)$$

$$J_v(\omega) = \frac{1}{K_1} \sum_{i=1}^{K_1} J_{v_i}(\omega) \quad (32)$$

and

$$I_{s_v}(\omega) = \frac{1}{MU_s} \frac{1}{K_1} \sum_{i=1}^{K_1} [X_{s_i}(\omega) X_{v_i}^*(\omega) + X_{s_i}^*(\omega) X_{v_i}(\omega)]. \quad (33)$$

From (10), (18), (19), (30), (31), (32), and (33) we have

$$E[J_{s_v}(\omega)] = \frac{1}{U_s K_1} \sum_{i=1}^{K_1} U_i \left(\frac{P_r}{B_s T}\right) + \frac{1}{K_1} \sum_{i=1}^{K_1} \left(\frac{b}{T}\right) = \frac{U_s^*}{U_s} \left(\frac{P_r}{B_s T}\right) + \frac{b}{T}, \quad \text{for } \omega \in (\omega_l, \omega_h) \quad (34)$$

where

$$U_s^* = \frac{1}{K_1} \sum_{i=1}^{K_1} U_i. \quad (35)$$

We note that $E[I_{s_v}(\omega)] = 0$ because $E[X_{s_i}(\omega) X_{v_i}^*(\omega)] = E[X_{s_i}(\omega)] E[X_{v_i}^*(\omega)] = 0$, and similarly, $E[X_{s_i}^*(\omega) X_{v_i}(\omega)] = 0$.

Since

$$C_1 = \sum_{k=k_l}^{k_h} J_{s_v}(k) \quad (36)$$

where k_l and k_h are the smallest and largest integers in $(f_l MT, f_h MT)$, respectively, and $J_{s_v}(k) = J_{s_v}(\omega = 2\pi k/M)$, the mean value of C_1 is

$$E[C_1] = k_s \left(\frac{U_s^* P_r}{U_s B_s T} + \frac{b}{T}\right) = M \left(\frac{f_h - f_l}{f_s}\right) \left(\frac{U_s^* P_r}{U_s B_s T} + \frac{b}{T}\right) = \frac{T_G B_s}{T} \left(\frac{U_s^* P_r}{U_s B_s} + b\right) \quad (37)$$

where $k_s = (k_h - k_l + 1) \cong T_G B_s$ and $T_G = MT$. Notice that $T_G B_s$ is not necessarily an integer. Therefore, there must be a roundoff error between $T_G B_s$ and k_s . In this paper, we neglect this minor issue.

From (30), we also have

$$\begin{aligned} \text{Cov}\{J_{s_v}(\omega_1), J_{s_v}(\omega_2)\} &= \text{Cov}\{J_s(\omega_1), J_s(\omega_2)\} \\ &+ \text{Cov}\{J_v(\omega_1), J_v(\omega_2)\} \\ &+ \text{Cov}\{I_{s_v}(\omega_1), I_{s_v}(\omega_2)\} \end{aligned} \quad (38)$$

because $J_s(\omega)$, $J_v(\omega)$, and $I_{s_v}(\omega)$ are mutually uncorrelated. From (11), the first and second terms of (38) can be written as

$$\begin{aligned} \text{Cov}\{J_s(\omega_1), J_s(\omega_2)\} &= \left(\frac{P_r}{K_1 U_s T_G B_s}\right)^2 \\ &\cdot \sum_{i=1}^{K_1} \sum_{j=1}^{K_1} |\Gamma_{ij}(\omega_1 - \omega_2)|^2 \\ &\omega_1, \omega_2 \in (\omega_l, \omega_h) \end{aligned} \quad (39)$$

and

$$\begin{aligned} \text{Cov}\{J_v(\omega_1), J_v(\omega_2)\} &= \left(\frac{b}{K_1 U_s T_G}\right)^2 \\ &\cdot \sum_{i=1}^{K_1} \sum_{j=1}^{K_1} |W_s(i-j, \omega_1 - \omega_2)|^2 \\ &\omega_1, \omega_2 \in (\omega_l, \omega_h) \end{aligned} \quad (40)$$

where $W_s(q, \omega)$ is the Fourier transform of

$$w_s(q, n) = w_s(n) w_s(n + qD_1). \quad (41)$$

The third term of (38) is given by (see Appendix III)

$$\begin{aligned} \text{Cov} \{I_{sv}(\omega_1), I_{sv}(\omega_2)\} &\equiv \left(\frac{P_r}{B_s}\right) b \left(\frac{1}{T_G U_s K_1}\right)^2 \\ &\sum_{i=1}^{K_1} \sum_{j=1}^{K_1} \{ \Gamma_{ij}(\omega_1 - \omega_2) W_s^*(i - j, \omega_1 - \omega_2) \\ &+ \Gamma_{ij}^*(\omega_1 - \omega_2) W_s(i - j, \omega_1 - \omega_2) \}. \end{aligned} \quad (42)$$

Substituting (39), (40), and (42) into (38) gives

$$\begin{aligned} \text{Cov} \{J_{sv}(\omega_1), J_{sv}(\omega_2)\} &= \left(\frac{P_r}{K_1 U_s T_G B_s}\right)^2 \\ &\cdot \sum_{i=1}^{K_1} \sum_{j=1}^{K_1} \left| \Gamma_{ij}(\omega_1 - \omega_2) \right. \\ &\left. + \frac{1}{\text{SNR}} W_s(i - j, \omega_1 - \omega_2) \right|^2, \\ &\text{for all } \omega_1, \omega_2 \in (\omega_l, \omega_h) \end{aligned} \quad (43)$$

where

$$\text{SNR} = \frac{P_r}{B_s b}. \quad (44)$$

Therefore, from (36) and (43) we see that

$$\begin{aligned} \text{Var} [C_1] &= E \left\{ \left(\sum_{k=k_l}^{k_h} J_{sv}(k) - E[J_{sv}(k)] \right)^2 \right\} \\ &= \sum_{k_1=k_l}^{k_h} \sum_{k_2=k_l}^{k_h} \text{Cov} \{J_{sv}(k_1), J_{sv}(k_2)\} \\ &= \frac{P_r^2}{(U_s K_1)^2 (T_G B_s)^2} \sum_{k_1=k_l}^{k_h} \sum_{k_2=k_l}^{k_h} \sum_{i=1}^{K_1} \sum_{j=1}^{K_1} \\ &\cdot \left| \Gamma_{ij}(k_1 - k_2) + \frac{1}{\text{SNR}} W_s(i - j, k_1 - k_2) \right|^2 \\ &= \frac{P_r^2}{(U_s K_1)^2 T_G B_s} \sum_{k=-k_s}^{k_s} \sum_{i=1}^{K_1} \sum_{j=1}^{K_1} \\ &\cdot \left| \Gamma_{ij}(k) + \frac{1}{\text{SNR}} W_s(i - j, k) \right|^2 \left(1 - \frac{|k|}{k_s}\right) \end{aligned} \quad (45)$$

where $\Gamma_{ij}(k) = \Gamma_{ij}(\omega = 2\pi k/M)$ and $W_s(i, k) = W_s(i, \omega = 2\pi k/M)$.

B. Mean and Variance of C_2

For the bottom path of Fig. 2, only noise is present. The mean and variance of C_2 can be directly obtained from (37), (44), and (45) by letting $P_r \rightarrow 0$, and setting $K_1 = K_2$, $W_s(q, k) = W_N(q, k)$, $M = N$ and $B_s = B_N$, i.e.

$$E[C_2] = k_s \left(\frac{b}{T}\right) = N \left(\frac{f_h}{f_s} - \frac{f_l}{f_s}\right) \left(\frac{b}{T}\right) = T_N B_N \left(\frac{b}{T}\right) \quad (46)$$

$$\begin{aligned} \text{Var} [C_2] &= \left(\frac{b}{U_N}\right)^2 \left(\frac{B_N}{T_N}\right) \frac{1}{K_2} \sum_{k=-k_s}^{k_s} \sum_{q=-K_2}^{K_2} |W_N(q, k)|^2 \\ &\cdot \left(1 - \frac{|q|}{K_2}\right) \left(1 - \frac{|k|}{k_s}\right) \end{aligned} \quad (47)$$

where

$$U_N = \frac{1}{N} \sum_{n=0}^{N-1} w_N^2(n). \quad (48)$$

$W_N(q, \omega)$ is the Fourier transform of

$$w_N(q, n) = w_N(n) w_N(n + qD_2). \quad (49)$$

$W_N(q, k) = W_N(q, \omega = 2\pi k/N)$, $T_N = NT$, $k_s = k_h - k_l + 1 = T_N B_N$, and k_l and k_h are the smallest and largest integers in $(f_l NT, f_h NT)$.

C. K_p of an Unbiased Estimate of P_r

From (37) and (46) one can form an unbiased estimate for P_r , as

$$\hat{P}_r = \frac{U_s T}{U_s^* T_G} \left(C_1 - \frac{T_G B_s}{T_N B_N} C_2 \right). \quad (50)$$

Note that $T_G = MT$ and $T_N = NT$ denote the time interval of one data segment for the top and the bottom signal path in Fig. 2, respectively.

Finally, we have

$$\text{Var} [\hat{P}_r] = \left(\frac{U_s T}{U_s^* T_G}\right)^2 \left\{ \text{Var} (C_1) + \left(\frac{T_G B_s}{T_N B_N}\right)^2 \text{Var} (C_2) \right\}. \quad (51)$$

Combining (45), (47), and (51), and substituting into (12) leads to the expression for K_p as follows:

$$\begin{aligned} K_p &= \frac{1}{\sqrt{T_G B_s}} \left(\frac{1}{M U_s^*}\right) \left\{ \frac{1}{K_1^2} \left[\sum_{k=-k_s}^{k_s} \sum_{i=1}^{K_1} \sum_{j=1}^{K_1} \right. \right. \\ &\cdot \left| \Gamma_{ij}(k) + \frac{1}{\text{SNR}} W_s(i - j, k) \right|^2 \left(1 - \frac{|k|}{k_s}\right) \\ &+ \frac{1}{K_2} \left(\frac{T_G B_s}{T_N B_N}\right) \left(\frac{M U_s}{N U_N}\right)^2 \frac{1}{\text{SNR}^2} \left[\sum_{k=-k_s}^{k_s} \sum_{q=-K_2}^{K_2} \right. \\ &\cdot \left. \left. |W_N(q, k)|^2 \left(1 - \frac{|k|}{k_s}\right) \left(1 - \frac{|q|}{K_2}\right) \right] \right\}^{1/2}. \end{aligned} \quad (52)$$

The resulting K_p equation appears to be complicated. However, we will consider two particular examples in the next section. One of these examples shows that this expression reduces to the well-known analog K_p equation. The other example shows that this expression reduces to the normalized standard deviation of Welch's power spectrum estimate when $k_s = 1$ and $\text{SNR} = \infty$.

IV. EXAMPLES OF EVALUATING THE DIGITAL K_p EQUATION

The first example is for $K_1 = K_2 = 1$, $(T_G/T_s) \ll k$, $< M/2$, $w_s(n)$, and $w_N(n)$ are rectangular windows. This case should correspond to the analog filter processor. For this example, $U_s = U_N = 1$, $U_s^* = T_s/T_G$, $W_s(0, 0) = M$, $W_N(0, 0) = N$, $\Gamma_{11}(0) = MT_s/T_G$, and

$$\sum_{k=0}^{M-1} \frac{|\Gamma_{11}(k)|^2}{M^2} = \sum_{n=0}^{M-1} \frac{\gamma_{11}^2(n)}{M} = \frac{T_s}{T_G}$$

The K_p is then

$$\begin{aligned} K_p &= \frac{1}{\sqrt{T_G B_s}} \frac{T_G}{MT_s} \left\{ \sum_{k=0}^{M-1} |\Gamma_{11}(k)|^2 + \frac{1}{\text{SNR}^2} |W_s(0, 0)|^2 \right. \\ &\quad \left. + \frac{2}{\text{SNR}} \Gamma_{11}(0) W_s(0, 0) \right. \\ &\quad \left. + \left(\frac{T_G B_s}{T_N B_N} \right) \left(\frac{M}{N} \right)^2 \frac{1}{\text{SNR}^2} |W_N(0, 0)|^2 \right\}^{1/2} \\ &= \frac{1}{\sqrt{T_G B_s}} \frac{T_G}{MT_s} \left\{ M^2 \left(\frac{T_s}{T_G} \right) + \frac{M^2}{\text{SNR}^2} \right. \\ &\quad \left. + \frac{2}{\text{SNR}} M^2 \frac{T_s}{T_G} + \frac{1}{\text{SNR}^2} M^2 \frac{T_G B_s}{T_N B_N} \right\}^{1/2} \\ &= \frac{1}{\sqrt{T_s B_s}} \left\{ 1 + \frac{2}{\text{SNR}} + \frac{1}{\text{SNR}^2} \left(\frac{T_G}{T_s} \right) \left(1 + \frac{T_G B_s}{T_N B_N} \right) \right\}^{1/2} \end{aligned} \quad (53)$$

Equation (53) is exactly the analog filter expression derived in [7] (also see [3]). This example provides a connection of the K_p equations for analog and digital signal processors.

As a second example, we examine the K_p equation for $T_G = T_s = T_N$, $D_1 = D_2$, $B_s = B_N$, $K_1 = K_2 = K$. Thus, $M = N$ and $U_s = U_N = U_s^*$ and $\Gamma_{ij}(k) = W_s(i - j, k) = W_N(i - j, k)$. Equation (52) then reduces to

$$\begin{aligned} K_p &= \frac{1}{\sqrt{k_s}} \frac{1}{MU_s} \frac{1}{\sqrt{K}} \left(1 + \frac{2}{\text{SNR}} + \frac{2}{\text{SNR}^2} \right)^{1/2} \\ &\quad \cdot \left\{ \sum_{k=-K}^{K} \sum_{q=-K}^K |W_s(q, k)|^2 \right. \\ &\quad \left. \cdot \left(1 - \frac{|k|}{k_s} \right) \left(1 - \frac{|q|}{K} \right) \right\}^{1/2} \end{aligned} \quad (54)$$

We will discuss two special cases for this example.

Case I. Assume that $k_s = 1$ and $\text{SNR} = \infty$. The resulting K_p should correspond to the normalized standard deviation of Welch's power spectrum estimate. First, let us consider the nonoverlapping case where $W_s(q, k) = 0$ for $q \neq 0$. The K_p equation (54) can be further reduced to

$$\begin{aligned} K_p &= \frac{1}{MU_s} \frac{1}{\sqrt{K}} |W_s(0, 0)| \\ &= \frac{1}{MU_s} \frac{1}{\sqrt{K}} \left(\sum_{n=0}^{M-1} w_s^2(n) \right) = \frac{1}{\sqrt{K}} \end{aligned} \quad (55)$$

which was also shown by Welch [6].

Second, let us consider the 50-percent overlapping case ($D = M/2$). In this case, $W_s(q, k) = 0$ for $q > 1$. Equation (54) can be expressed as

$$\begin{aligned} K_p &= \frac{1}{MU_s} \frac{1}{\sqrt{K}} \left\{ |W_s(0, 0)|^2 + 2 \right. \\ &\quad \left. \cdot \left(1 - \frac{1}{K} \right) |W_s(1, 0)|^2 \right\}^{1/2} \end{aligned} \quad (56)$$

Following an example in Welch's paper, we examine the case with the following window function:

$$\begin{aligned} w_s(n) &= 1 - \left(\frac{n - \frac{M-1}{2}}{\frac{M+1}{2}} \right)^2 \\ &0 \leq n \leq M-1. \end{aligned} \quad (57)$$

For this case

$$|W_s(1, 0)|^2 \cong \frac{1}{9} |W_s(0, 0)|^2$$

Therefore

$$\begin{aligned} K_p &= \frac{1}{MU_s} \frac{1}{\sqrt{K}} \left(\frac{11}{9} - \frac{2}{9K} \right)^{1/2} |W_s(0, 0)| \\ &\cong \frac{1}{MU_s} \frac{1}{\sqrt{K}} \left(\frac{11}{9} \right)^{1/2} |W_s(0, 0)| = \left(\frac{11}{9} \right)^{1/2} \frac{1}{\sqrt{K}} \end{aligned} \quad (58)$$

which is the same as the results shown in [6]. As previously stated, Welch's power spectrum estimation results are special cases of the derived K_p equation.

Case II. Assume that $w_s(n)$ is a generalized Hamming window given by

$$\begin{aligned} w_s(n) &= \alpha - (1 - \alpha) \cos \left(\frac{2\pi n}{M} \right), \\ &0 \leq n \leq M-1. \end{aligned} \quad (59)$$

Note that it is a rectangular window (i.e., no weight) for $\alpha = 1$, and a Hamming window for $\alpha = 0.5$. $W_s(0, k)$ can be easily shown to be

$$W_s(0, k) = \begin{cases} (\alpha^2 + \frac{1}{2}(1 - \alpha)^2)M, & k = 0 \\ -\alpha(1 - \alpha)M, & k = 1, M-1 \\ \frac{1}{2}(1 - \alpha)^2 M, & k = 2, M-2 \\ 0, & \text{otherwise} \end{cases} \quad (60)$$

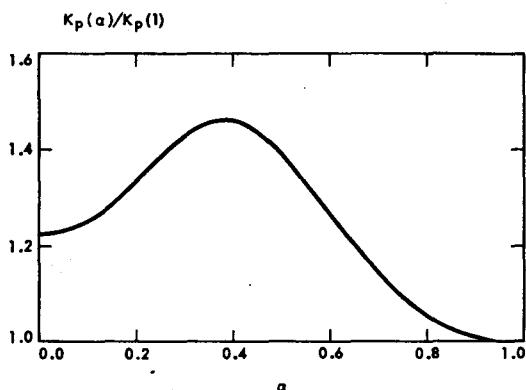


Fig. 3. $K_p(\alpha)/K_p(1)$ for a generalized Hamming window for one data segment.

and $U_s = W_s(0, 0)/M = \alpha^2 + \frac{1}{2}(1 - \alpha)^2$. First, let us consider the case $K = 1$ and $2 \ll k_s < M/2$. For this special case, (54) can be reduced to

$$\begin{aligned}
 K_p &= \frac{1}{\sqrt{k_s}} \frac{1}{MU_s} \left(1 + \frac{2}{\text{SNR}} + \frac{2}{\text{SNR}^2} \right)^{1/2} \\
 &\quad \cdot \left\{ \sum_{k=0}^{M-1} |W_s(0, k)|^2 \right\}^{1/2} \\
 &= \frac{1}{\sqrt{k_s}} \frac{(\alpha^4 + 3\alpha^2(1 - \alpha)^2 + \frac{3}{8}(1 - \alpha)^4)^{1/2}}{\alpha^2 + \frac{1}{2}(1 - \alpha)^2} \\
 &\quad \cdot \left(1 + \frac{2}{\text{SNR}} + \frac{2}{\text{SNR}^2} \right)^{1/2} \quad (61)
 \end{aligned}$$

The ratio of $K_p(\alpha)$ to $K_p(1)$ versus α is plotted in Fig. 3. This verifies that, indeed, as mentioned in the introduction, the use of windows increases K_p and therefore degrades system performance.

Next, we consider the overlapping case with $\text{SNR} = 1$, $M = 256$, and $L = 1024$. We directly compute K_p using (54) for $K = 4$ with nonoverlapping, $K = 5$ with 25-percent overlapping, $K = 7$ with 50-percent overlapping, $K = 13$ with 75-percent overlapping data segment, and $K = 25$ with 87.5-percent overlapping data segment. The resulting K_p 's (as function of α) are shown in Fig. 4(a)–(d) for $k_s = 1, 2, 4$, and 64 , respectively. Note that the σ_0 cells associated with $k_s = 1, 2$, and 4 are much smaller than the σ_0 cell associated with $k_s = 64$ because $B_s = k_s f_s / M$. From Fig. 4(a) we see that K_p does not depend on the window for the nonoverlapping case when $k_s = 1$. Data segment overlapping improves K_p . The amount of improvement depends on the window chosen. Notice that when $k_s = 1$ the correlation between frequency bins due to windowing and data segment overlapping does not appear in the K_p equation. When $k_s > 1$, the correlation between frequency bins due to windowing and data seg-

ment overlapping may actually degrade K_p (see Fig. 4(b)–(d)).

Finally, we consider K_p versus the percentage in data segment overlap for $\text{SNR} = 1$, $M = 256$, $L = 8192$, $k_s = 4$, and $\alpha = 0.5$ (Hamming window). The result is shown in Fig. 5. From this figure we see that K_p decreases as the amount of overlap increases and approaches an asymptote for overlap greater than 50 percent. In other words, little improvement in K_p is obtained when the amount of overlapping is more than 50 percent.

We note that a generalized Hamming window is very narrow in the frequency domain because only three values are nonzero for $0 \leq k \leq M - 1$. The hardware required to implement the generalized Hamming window can be quite simple because it only involves three frequency bins for convolution in the frequency domain.

V. DISCUSSION

A digital Doppler processor is planned for on-board digital signal processing for NSCAT. In this paper, we have derived an expression for the normalized standard deviation of backscatter power measurements K_p for such a digital signal processor. The effects of two digital signal processing techniques, namely windowing and data segment overlap processing, are treated. Windowing must be invoked in cases where spectral leakage is to be minimized in order to avoid inter- σ_0 cell interference. When windowing is used, overlap processing may then be considered to minimize the system performance degradation due to the windowing. Although the resulting expression for K_p is quite complex, we have demonstrated that it reduces to the well-known K_p expression for analog signal processors and that Welch's power spectrum estimation results [6] are special cases of the derived K_p expression.

In the NSCAT baseline design, a Hamming window and 50-percent overlap processing will be used. The Hanning window, applied through convolution in frequency domain, was chosen because it minimizes spectral leakage and is simple to implement. In fact, since the window weights are $\frac{1}{2}$ and $\frac{1}{4}$, only bit shifting, addition and subtraction are required without any multiplication. This lessens the computation load in a spaceborne processor. Based on K_p values versus computational load, a 50-percent overlap was chosen for the baseline design (see Fig. 5). There are on-going efforts to refine this baseline design using the K_p expression.

In addition to utilizing a digital signal processor to improve system performance, NSCAT also plans to use six antennas in contrast to the four antennas on SASS. Each side of the subsatellite track will be illuminated by three antennas. They will provide three different azimuthal observations of σ_0 from the ocean for wind vector estimation. This will simplify data interpretation by reducing the number of ambiguities in the estimated wind direction (see [3] and [9]).

Details of the NSCAT design, as well as further trade-offs in the digital Doppler processors will be reported in future papers.

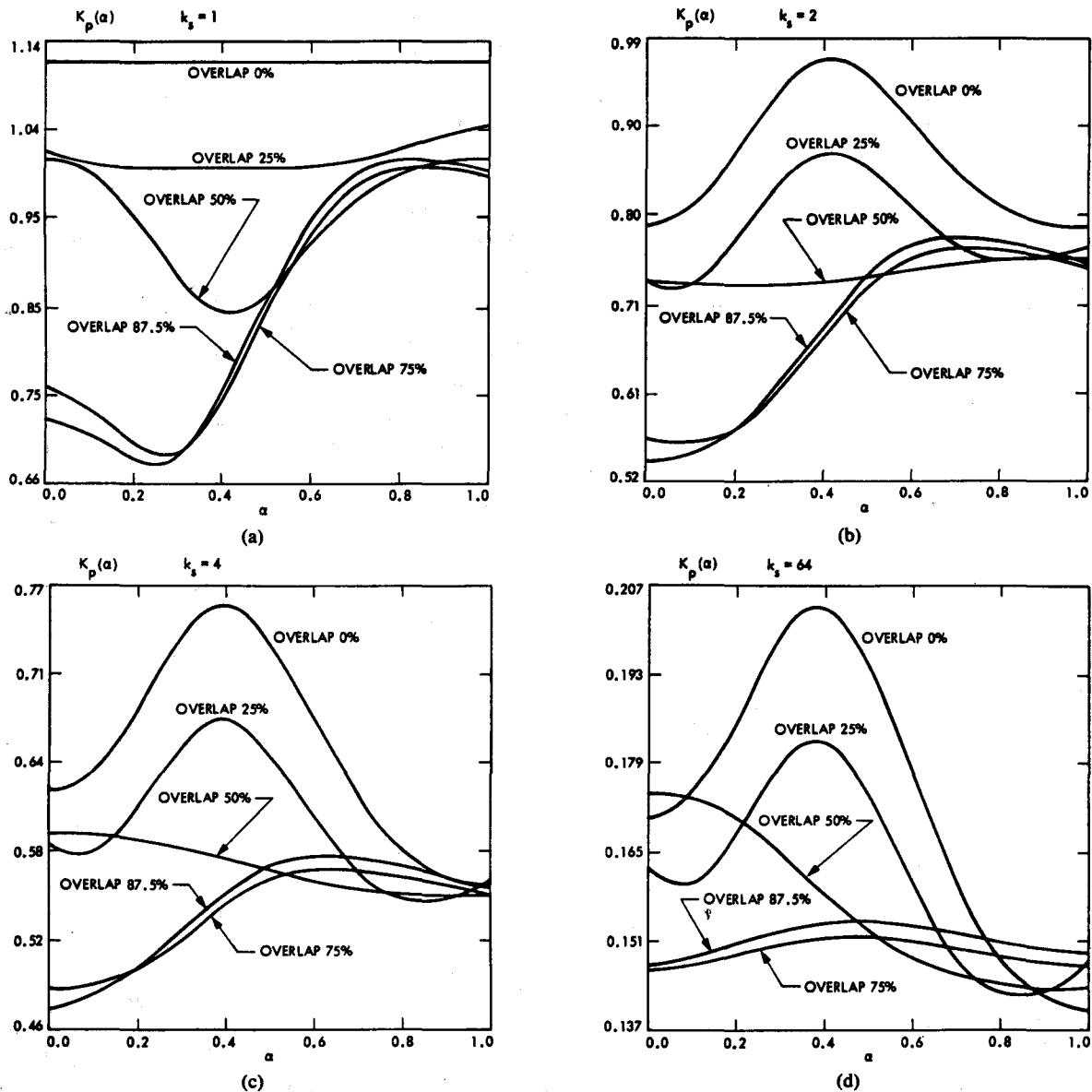


Fig. 4: $K_p(\alpha)$ for a generalized Hamming window and overlapping and nonoverlapping segments for (a) $k_s = 1$, (b) $k_s = 2$, (c) $k_s = 4$, and (d) $k_s = 64$, respectively.

APPENDIX I

PROOF OF EQUATION (11)

From (4) we have

$$\begin{aligned}
 & E\{J_i(\omega_1) J_r(\omega_2)\} \\
 &= \left(\frac{1}{MU_i}\right) \left(\frac{1}{MU_r}\right) \\
 &\cdot E \left\{ \sum_k \sum_l \sum_m \sum_n x_i(k) x_i(l) x_r(m) x_r(n) \right. \\
 &\cdot \gamma_i(k) \gamma_i(l) \gamma_r(m) \gamma_r(n) \\
 &\cdot \left. \exp(j[\omega_1(k-l) + \omega_2(m-n)]) \right\}. \quad (A1)
 \end{aligned}$$

For a zero-mean stationary Gaussian process $x(n)$, it is well known that

$$\begin{aligned}
 & E[x_i(k) x_i(l) x_r(m) x_r(n)] \\
 &= E[x_i(k) x_i(l)] E[x_r(m) x_r(n)] \\
 &\quad + E[x_i(k) x_r(m)] E[x_i(l) x_r(n)] \\
 &\quad + E[x_i(k) x_r(n)] E[x_i(l) x_r(m)] \\
 &= \phi_x(l-k) \phi_x(n-m) \\
 &\quad + \phi_x(k-m+qD) \phi_x(l-n+qD) \\
 &\quad + \phi_x(k-n+qD) \phi_x(l-m+qD) \quad (A2)
 \end{aligned}$$

where $\phi_x(k)$ is the correlation function of $x(n)$, and

$$q = i - r. \quad (A3)$$

Thus

$$E\{J_i(\omega_1) J_r(\omega_2)\} = Q_1 + Q_2 + Q_3 \quad (A4)$$

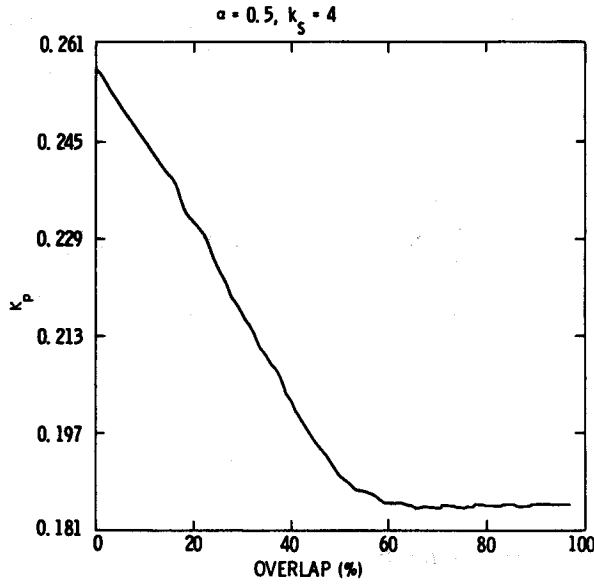


Fig. 5. K_p versus overlapping for $k_s = 4$ and $\alpha = 0.5$.

where

$$Q_1 = \left(\frac{1}{MU_i}\right) \left(\frac{1}{MU_r}\right) \left\{ \sum_k \sum_l \sum_m \sum_n \right. \\ \cdot \phi_x(l-k) \phi_x(n-m) \gamma_i(k) \gamma_i(l) \gamma_r(m) \gamma_r(n) \\ \cdot \exp [j[\omega_1(k-l) + \omega_2(m-n)]] \left. \right\} \quad (A5)$$

$$Q_2 = \left(\frac{1}{MU_i}\right) \left(\frac{1}{MU_r}\right) \sum_k \sum_l \sum_m \sum_n \\ \cdot \{ \phi_x(k-m+qD) \\ \cdot \phi_x(l-n+qD) \gamma_i(k) \gamma_i(l) \gamma_r(m) \gamma_r(n) \\ \cdot \exp [j[\omega_1(k-l) + \omega_2(m-n)]] \} \quad (A6)$$

and

$$Q_3 = \left(\frac{1}{MU_i}\right) \left(\frac{1}{MU_r}\right) \sum_k \sum_l \sum_m \sum_n \\ \cdot \{ \phi_x(k-n+qD) \phi_x(l-m+qD) \\ \cdot \gamma_i(k) \gamma_i(l) \gamma_r(m) \gamma_r(n) \\ \cdot \exp [j[\omega_1(k-l) + \omega_2(m-n)]] \}. \quad (A7)$$

We now derive Q_1 , Q_2 , and Q_3 . Because the power density spectrum $P_x(\omega)$ of $x(n)$ is the Fourier transform of $\phi_x(n)$, Q_1 can be expressed in frequency domain

$$Q_1 = \left(\frac{1}{MU_i}\right) \left(\frac{1}{MU_r}\right) \sum_k \sum_l \sum_m \sum_n \\ \cdot \left\{ \left(\frac{1}{2\pi}\right)^2 \int_{-\pi}^{\pi} P_x(\theta_1) \exp [j\theta_1(l-k)] d\theta_1 \right. \\ \cdot \left. \int_{-\pi}^{\pi} P_x(\theta_2) \exp [j\theta_2(n-m)] \right.$$

$$\cdot d\theta_2 \gamma_i(k) \gamma_i(l) \gamma_r(m) \gamma_r(n) \\ \cdot \left. \exp [j[\omega_1(k-l) + \omega_2(m-n)]] \right\} \\ = \left(\frac{1}{MU_i}\right) \left(\frac{1}{MU_r}\right) \left\{ \left(\frac{1}{2\pi}\right)^2 \int_{-\pi}^{\pi} \int_{-\pi}^{\pi} P_x(\theta_1) P_x(\theta_2) \right. \\ \cdot \sum_k \sum_l \sum_m \sum_n \gamma_i(k) \gamma_i(l) \gamma_r(m) \gamma_r(n) \\ \cdot \exp [-j(\omega_1 - \theta_1)(l-k)] \\ \cdot \exp [-j(\omega_2 - \theta_2)(n-m)] d\theta_1 d\theta_2 \left. \right\} \\ = \left(\frac{1}{MU_i}\right) \left(\frac{1}{MU_r}\right) \left(\frac{1}{2\pi}\right)^2 \\ \cdot \int_{-\pi}^{\pi} \int_{-\pi}^{\pi} P_x(\theta_1) P_x(\theta_2) |\Gamma_r(\omega_1 - \theta_1)|^2 \\ \cdot |\Gamma_r(\omega_2 - \theta_2)|^2 d\theta_1 d\theta_2 \\ = E[J_r(\omega_1)] E[J_r(\omega_2)]. \quad (A8)$$

Therefore

$$\text{Cov} \{J_i(\omega_1), J_r(\omega_2)\} = Q_2 + Q_3. \quad (A9)$$

From (A6) we have

$$Q_2 = \left(\frac{1}{MU_i}\right) \left(\frac{1}{MU_r}\right) \left(\frac{1}{2\pi}\right)^2 \\ \cdot \left\{ \int_{-\pi}^{\pi} \int_{-\pi}^{\pi} P_x(\theta_1) P_x(\theta_2) \sum_k \sum_l \sum_m \sum_n \right. \\ \cdot \gamma_i(k) \gamma_i(l) \gamma_r(m) \gamma_r(n) \cdot \exp [j[\theta_1(k-m) \\ + \theta_2(l-n) + \omega_1(k-l) + \omega_2(m-n)]] \\ \cdot \exp [j(\theta_1 + \theta_2) qD] d\theta_1 d\theta_2 \left. \right\} \\ = \left(\frac{1}{MU_i}\right) \left(\frac{1}{MU_r}\right) \left(\frac{1}{2\pi}\right)^2 \left\{ \int_{-\pi}^{\pi} \int_{-\pi}^{\pi} P_x(\theta_1) P_x(\theta_2) \right. \\ \cdot \Gamma_i^*(\theta_1 + \omega_1) \Gamma_i^*(\theta_2 - \omega_1) \Gamma_r(\theta_1 - \omega_2) \\ \cdot \Gamma_r(\theta_2 + \omega_2) \cdot \exp [j(\theta_1 + \theta_2) qD] d\theta_1 d\theta_2 \left. \right\} \\ = \left(\frac{1}{MU_i}\right) \left(\frac{1}{MU_r}\right) \left(\frac{1}{2\pi}\right)^2 \left\{ \int_{-\pi}^{\pi} P_x(\theta_1) \Gamma_i^*(\theta_1 + \omega_1) \right. \\ \cdot \Gamma_r(\theta_1 - \omega_2) \exp [j\theta_1 qD] d\theta_1 \left. \right\} \\ \cdot \left\{ \int_{-\pi}^{\pi} P_x(\theta_2) \Gamma_i^*(\theta_2 - \omega_1) \Gamma_r(\theta_2 + \omega_2) \right. \\ \cdot \exp [j\theta_2 qD] d\theta_2 \left. \right\}.$$

$$\begin{aligned}
&\equiv \left(\frac{1}{MU_i}\right) \left(\frac{1}{MU_j}\right) P^2 \left\{ \frac{1}{2\pi} \int_{-\pi}^{\pi} \Gamma_i^*(\theta_1 + \omega_1) \right. \\
&\quad \cdot \Gamma_r(\theta_1 - \omega_2) \exp [j\theta_1 q D] d\theta_1 \left. \right\} \\
&\quad \cdot \left\{ \frac{1}{2\pi} \int_{-\pi}^{\pi} \Gamma_i^*(\theta_2 - \omega_1) \Gamma_r(\theta_2 + \omega_2) \right. \\
&\quad \cdot \exp [j\theta_2 q D] d\theta_2 \left. \right\} \\
&= \left(\frac{1}{MU_i}\right) \left(\frac{1}{MU_j}\right) P^2 |\Gamma_{ir}(\omega_1 + \omega_2)|^2, \\
&\quad \text{(since (B1)) for } \omega_1, \omega_2 \in (\omega_a, \omega_b). \quad (A10)
\end{aligned}$$

Similarly, we can show

$$\begin{aligned}
Q_3 &\equiv \left(\frac{1}{MU_i}\right) \left(\frac{1}{MU_r}\right) \left(\frac{1}{2\pi}\right)^2 P^2 \left\{ \int_{-\pi}^{\pi} \Gamma_i^*(\theta_1 + \omega_1) \right. \\
&\quad \cdot \Gamma_r(\theta_1 + \omega_2) \exp [j\theta_1 q D] d\theta_1 \left. \right\} \\
&\quad \cdot \left\{ \int_{-\pi}^{\pi} \Gamma_i^*(\theta_2 - \omega_1) \Gamma_r(\theta_2 - \omega_2) \exp [j\theta_2 q D] d\theta_2 \right\} \\
&= \left(\frac{1}{MU_i}\right) \left(\frac{1}{MU_r}\right) P^2 |\Gamma_{ir}(\omega_1 - \omega_2)|^2, \\
&\quad \text{for } \omega_1, \omega_2 \in (\omega_a, \omega_b). \quad (A11)
\end{aligned}$$

Thus

$$\begin{aligned}
&\text{Cov} \{J_i(\omega_1), J_r(\omega)\} \\
&= \left(\frac{1}{MU_i}\right) \left(\frac{1}{MU_r}\right) P^2 \\
&\quad \cdot \{|\Gamma_{ir}(\omega_1 + \omega_2)|^2 + |\Gamma_{ir}(\omega_1 - \omega_2)|^2\} \\
&\equiv \left(\frac{1}{MU_i}\right) \left(\frac{1}{MU_r}\right) P^2 |\Gamma_{ir}(\omega_1 - \omega_2)|^2. \quad (A12)
\end{aligned}$$

Therefore

$$\begin{aligned}
\text{Cov} \{J(\omega_1), J(\omega_2)\} &\equiv \frac{1}{K^2} \left(\frac{P^2}{M^2}\right) \sum_{i=1}^K \sum_{j=1}^K \\
&\quad \cdot \left[\frac{1}{U_i} \frac{1}{U_j} |\Gamma_{ij}(\omega_1 - \omega_2)|^2 \right]. \quad (A13)
\end{aligned}$$

APPENDIX II AN INTEGRAL EQUATION

In this appendix, we prove the following identity equation:

$$\begin{aligned}
&\frac{1}{2\pi} \int_{-\pi}^{\pi} \Gamma_i^*(\theta - \omega_1) \Gamma_r(\theta + \omega_2) \exp [j\theta q D] d\theta \\
&= \Gamma_{ir}(\omega_1 + \omega_2) \exp [-j\omega_2 q D] \quad (B1)
\end{aligned}$$

where $\Gamma_i(\omega)$, $\Gamma_{ir}(\omega)$, and $\Gamma_r(\omega)$ are the Fourier transforms of $\gamma_i(n)$, $\gamma_r(n)$, and $\gamma_{ir}(n)$ (see (7)), respectively, and $q = i - r$.

Proof:

$$\begin{aligned}
&\frac{1}{2\pi} \int_{-\pi}^{\pi} \Gamma_i^*(\theta - \omega_1) \Gamma_r(\theta + \omega_2) \exp [j\theta q D] d\theta \\
&= \frac{1}{2\pi} \int_{-\pi}^{\pi} \Gamma_i(\omega_1 - \theta) \Gamma_r(\theta + \omega_2) \exp [j\theta q D] d\theta \\
&= \frac{1}{2\pi} \int_{-\pi}^{\pi} \Gamma_i(\omega_1 + \omega_2 - y) \Gamma_r(y) \\
&\quad \cdot \exp [j(y - \omega_2) q D] dy \\
&= \frac{1}{2\pi} \left\{ \int_{-\pi}^{\pi} \Gamma_i(\omega_1 + \omega_2 - y) \Gamma_r(y) \right. \\
&\quad \cdot \exp [jy q D] dy \left. \right\} \exp [-j\omega_2 q D] \\
&= \Gamma_i(\omega) * (\Gamma_r(\omega) \exp [j\omega q D])|_{\omega=\omega_1+\omega_2} \exp [-j\omega_2 q D] \\
&= \Gamma_{ir}(\omega_1 + \omega_2) \exp [-j\omega_2 q D].
\end{aligned}$$

APPENDIX III PROOF OF EQUATION (42)

Proof: From (33) we have

$$\begin{aligned}
&\text{Cov} \{I_{sr}(\omega_1), I_{sr}(\omega_2)\} \\
&= \left(\frac{1}{MU_s K_1}\right)^2 \sum_{i=1}^{K_1} \sum_{r=1}^{K_1} 2 \text{Re} \{E[X_{s_i}(\omega_1) X_{s_r}(\omega_2)] \\
&\quad \cdot E[X_{s_i}^*(\omega_1) X_{s_r}^*(\omega_2)] + E[X_{s_i}(\omega_1) X_{s_r}^*(\omega_2)] \\
&\quad \cdot E[X_{s_r}(\omega_1) X_{s_i}(\omega_2)]\}. \quad (C1)
\end{aligned}$$

To further simplify (C1), we need to derive $E[X_{s_i}(\omega_1) X_{s_r}^*(\omega_2)]$ as follows:

$$\begin{aligned}
E[X_{s_i}(\omega_1) X_{s_r}^*(\omega_2)] &= E \left\{ \sum_{m=0}^{M-1} \sum_{n=0}^{M-1} s(n + (i-1)D_1) \right. \\
&\quad \cdot \gamma_i(n) s(m + (r-1)D_1) \gamma_r(m) \\
&\quad \cdot \exp [-j(\omega_1 n - \omega_2 m)] \left. \right\} \\
&= \sum_{m=0}^{M-1} \sum_{n=0}^{M-1} \phi_s(n - m + (i-r)D_1) \\
&\quad \cdot \gamma_i(n) \gamma_r(m) \exp [-j(\omega_2 n - \omega_2 m)] \\
&= \sum_{m=0}^{M-1} \sum_{n=0}^{M-1} \left(\frac{1}{2\pi}\right) \int_{-\pi}^{\pi} P_s(\theta) \\
&\quad \cdot \exp [j(n - m + (i-r)D_1)\theta] \\
&\quad \cdot \exp [-j(\omega_1 n - \omega_2 m)] \gamma_i(n) \gamma_r(m) d\theta
\end{aligned}$$

$$\begin{aligned}
E[X_{si}(\omega_1) X_{sj}^*(\omega_2)] &= \frac{1}{2\pi} \int_{-\pi}^{\pi} P_s(\theta) \Gamma_i^*(\theta - \omega_1) \\
&\quad \cdot \Gamma_r(\theta - \omega_2) \exp [j(i - r)D_1\theta] d\theta \\
&= \frac{P_r}{B_s T} \left(\frac{1}{2\pi} \right) \int_{-\pi}^{\pi} \Gamma_i^*(\theta - \omega_1) \\
&\quad \cdot \Gamma_r(\theta - \omega_2) \exp [j(i - r)D_1\theta] d\theta \\
&= \frac{P_r}{B_s T} \Gamma_{ir}(\omega_1 - \omega_2) \exp [j\omega_2(i - r)D_1], \\
&\quad \text{(from (B1)) for } \omega_1, \omega_2 \in (\omega_l, \omega_h).
\end{aligned} \tag{C2}$$

Similarly, one can easily show that

$$\begin{aligned}
E[X_{sr}(\omega_1) X_{ss}(\omega_2)] &= \frac{P_r}{B_s T} \Gamma_{ir}(\omega_1 + \omega_2) \\
&\quad \cdot \exp [-j\omega_2(i - r)D_1] \\
&\quad \omega_1, \omega_2 \in (\omega_l, \omega_h)
\end{aligned} \tag{C3}$$

$$\begin{aligned}
E[X_{sr}^*(\omega_1) X_{sr}^*(\omega_2)] &= \left(\frac{b}{T} \right) W_s^*(i - r, \omega_1 + \omega_2) \\
&\quad \cdot \exp [j\omega_2(i - r)D_1] \\
&\quad \omega_1, \omega_2 \in (\omega_l, \omega_h),
\end{aligned} \tag{C4}$$

and

$$\begin{aligned}
E[X_{sr}^*(\omega_1) X_{sr}(\omega_2)] &= \left(\frac{b}{T} \right) W_s^*(i - r, \omega_1 - \omega_2) \\
&\quad \cdot \exp [-j\omega_2(i - r)D_1] \\
&\quad \omega_1, \omega_2 \in (\omega_l, \omega_h).
\end{aligned} \tag{C5}$$

Substituting (C2) through (C5) into (C1) gives

$$\begin{aligned}
\text{Cov} \{I_{sr}(\omega_1), I_{sr}(\omega_2)\} \\
&= 2 \left(\frac{P_r}{B_s} \right) b \left(\frac{1}{T_G U_s K_1} \right)^2 \\
&\quad \cdot \sum_{i=1}^{K_1} \sum_{r=1}^{K_1} \text{Re} \{ \Gamma_{ir}(\omega_1 - \omega_2) W_s^*(i - r, \omega_1 - \omega_2) \\
&\quad + \Gamma_{ir}(\omega_1 + \omega_2) W_s^*(i - r, \omega_1 + \omega_2) \} \\
&\equiv 2 \left(\frac{P_r}{B_s} \right) b \left(\frac{1}{T_G U_s K_1} \right)^2 \sum_{i=1}^{K_1} \sum_{r=1}^{K_1} \\
&\quad \cdot \text{Re} \{ \Gamma_{ir}(\omega_1 - \omega_2) W_s^*(i - r, \omega_1 - \omega_2) \}
\end{aligned} \tag{C6}$$

which implies (42).

REFERENCES

- [1] R. K. Moore and F. T. Ulaby, "The radar radiometer," *Proc. IEEE*, vol. 57, pp. 587-590, Apr. 1969.
- [2] W. L. Jones, L. C. Schroeder, D. H. Boggs, E. M. Bracalente, R. A. Brown, G. J. Dome, W. J. Pierson, and F. J. Wentz, "The Seasat-A satellite scatterometer: The geophysical evaluation of re-

motely sensed wind vectors over the ocean," *J. Geophys. Res.*, vol. 87, no. C5, pp. 3297-3317, 1982.

- [3] E. Bracalente, E. D. Boggs, W. Grantham, and J. Sweet, "The SASS scattering coefficient (σ_0) algorithm," *IEEE J. Ocean. Eng.*, vol. OE-5, Apr. 1980.
- [4] F. Li, P. Callahan, D. Lame, and C. Winn, "NASA scatterometer on NROSS—A system for global observations of oceanic winds," *Proc. IGARSS '84* (Strasbourg, France), Aug. 1984.
- [5] D. Long, C. Y. Chi, and F. Li, "Digital filter processor design for spaceborne scatterometers," *Proc. of IGARSS '84* (Strasbourg, France), Aug. 1984.
- [6] P. Welch, "The use of fast Fourier transform for the estimation of power spectra: A method based on time averaging over short, modified periodograms," *IEEE Trans. Audio Electroacoust.*, vol. AU-15, pp. 70-73, June 1967.
- [7] R. Fisher, "Standard deviation of scatterometer measurements from space," *IEEE Trans. Geosci. Electron.*, vol. GE-10, no. 2, pp. 106-113, Apr. 1972.
- [8] A. Oppenheim and R. Schaffer, *Digital Signal Processing*. Englewood Cliffs, NJ: Prentice-Hall, 1975.
- [9] L. C. Schroeder, W. L. Grantham, E. M. Bracalente, C. L. Britt, K. S. Shanmugan, F. J. Wentz, D. F. Wylie, and B. B. Hinton, "Removal of ambiguous wind directions for a Ku-band scatterometer using three different azimuth angles," *IEEE Trans. Geosci. Remote Sensing*, vol. GE-23, no. 2, pp. 91-100, Mar. 1985.
- [10] L. C. Schroeder, D. H. Boggs, G. Dome, I. M. Halbertam, W. L. Jones, W. J. Pierson, and F. J. Wentz, "The relationship between wind vector and normalized radar cross section used to derive SEASAT-A satellite scatterometer winds," *J. Geophys. Res.*, vol. 87, no. C5, pp. 3318-3336, Apr. 1982.



Chong-Yung Chi (S'83-M'83) was born in Taiwan, Republic of China, on August 7, 1952. He received the B.S. degree from the Tatung Institute of Technology in Taipei, Taiwan, in 1975, the M.S. degree from the National Taiwan University in Taipei, Taiwan, in 1977, and the Ph.D. degree from the University of Southern California at Los Angeles, in 1983, all in electrical engineering.

In September 1979, he was appointed a Teaching/Research Assistant, and later became a Research Assistant in the Department of Electrical

Engineering Systems at the University of Southern California. Since July 1983, he has been a member of the technical staff in the Radar Science and Engineering Section at the Jet Propulsion Laboratory at Pasadena, CA. Currently, he is engaged in studies of spaceborne radar scatterometer systems and radar image processing. His research interests include digital signal processing, system identification, and estimation theory.



David G. Long was born in Las Vegas, NV, on November 30, 1958. He received the B.S. and M.S. degrees in electrical engineering from Brigham Young University in 1982 and 1983, respectively. He is currently working toward the Ph.D. degree in electrical engineering at the University of Southern California, Los Angeles.

He is employed at the Jet Propulsion Laboratory in Pasadena as a member of the technical staff in the Radar Science and Engineering Section. His technical interests include digital signal processing,

speech analysis, and radar processing.

Mr. Long is a member of Tau Beta Pi, Eta Kappa Nu, and Sigma Xi and has served as vice-chairman of a student chapter of the IEEE.



Fuk-Kwok Li was born in Hong Kong in 1953. He received the B.Sc. and Ph.D. degrees in physics from the Massachusetts Institute of Technology in 1975 and 1979, respectively.

He joined the Jet Propulsion Laboratory, California Institute of Technology, in 1979, and has been involved in studies of spaceborne radar systems. He has developed a digital SAR processor/simulator, investigated the tradeoffs on various SAR image quality parameters, and developed several techniques for SAR Doppler parameter es-

timation. Since 1983, he has been involved in the design and development of ocean scatterometers. Presently, he is the Supervisor of the Radar Systems Science and Engineering Group.